

GT2011-45- (-

CFD ANALYSES OF HPT BLADE AIR DELIVERY SYSTEM WITH AND WITHOUT IMPELLERS

Charles Wu
Pratt & Whitney
400 Main Street, East Hartford, CT 06108
Email: charles.wu@pw.utc.com

Boris Vaisman
Currently at
Business School, Columbia University
Email: BVaisman12@gsb.columbia.edu

Kevin McCusker
Pratt & Whitney
400 Main Street, East Hartford, CT 06108
Email: kevin.mccusker@pw.utc.com

ABSTRACT

In the design of a HPT blade cooling air delivery system, sufficient supply pressure is required to guarantee HPT blades are working properly in the high temperature environment. A design goal is to set a pressure level at the blade inlet that will prevent the ingestion of gaspath air into the blades which is caused by pressure fluctuations under various operating conditions and other uncertainties.

Traditional 1-D design tools are not sophisticated enough for detailed system analysis. Therefore, CFD (Computational Fluid Dynamics) analysis was utilized for designing HPT blade cooling air delivery system to guarantee meeting the supply pressure requirement. Two HPT blade air delivery systems were explored. The baseline is a cooling air delivery system without radial impellers. It provides a simplistic design at low manufacturing cost, however CFD analysis shows that the system has a larger pressure loss at the broach slot entrance and delivers low supply pressure. The alternative is a cooling air delivery system with radial impellers. CFD analysis shows that the system with impellers results in much better aerodynamic performance at the broach slots and provides high supply pressure, but comes with the price of high manufacturing cost and lower TSFC due to the parasitic drag induced by impellers.

For the alternative approach, three high solidity impeller designs were analyzed. The alternative approaches analyzed had inlet angles of 0°, 30°, 90° and exit angles of 0°, respectively. Comparisons of detailed aerodynamic performance are presented in the paper. CFD simulation reveals that the source of pressure loss without impellers is caused by mismatch of the swirl ratio at broach slot entrance. CFD results show that a system with radial impellers produces a better matched swirl ratio at broach slot entrance. Radial impellers enhance aerodynamic performance and improve pressure distribution within broach slots.

NOMENCLATURE

HPT	High Pressure Turbine
TOBI	Tangential On-Board Injection
C	Blade or impeller chord
C_w	Non-dimensional flow rate $C_w = m/\mu R_{\text{disk}}$
m	Mass flow rate
r	Local radial distance
R	Gas constant
R_{disk}	Outer radius of the disk
Re_ϕ	Rotational Reynolds number $Re_\phi = \rho \Omega R_{\text{disk}}^2 / \mu$
s	Blade spacing
U_∞	Local free stream velocity
V_a	Axial velocity
V_ϕ	Tangential velocity
T	Temperature
TSFC	Thrust Specific Fuel Consumption
Y^+	Dimensionless wall distance $y^+ = \text{sqrt}(\rho \tau_w) r / \mu$
γ	Specific heat ratio
μ	Dynamic viscosity
ρ	Fluid Density
β	Swirl ratio or RPM factor $\beta = V_\phi / \Omega r$
Ω	Angular velocity

Subscripts

e	exit
i	inlet
s	Static
ϕ	Tangential component

1 INTRODUCTION

High pressure turbine blades of modern aircraft engines require cooling since they operate in an environment in which the gas path temperature is higher than metal melting

temperature- In this paper, the designs analyzed consist of a HPT second blade air delivery system. Since the cooling air is delivered from one rotating frame to another and without stationary parts involved, a TOBI-less cooling air delivery system is employed.

The pressure requirement is the primary concern in cooling air delivery system design. This design aims to set a sufficient supply pressure level at the broach slots of turbine blades to prevent blade burning. The sufficient supply pressure guarantees the targeted mass flow rate to ensure HPT blades are cooled properly in the high temperature environment regardless of the fluctuations in operating conditions and other uncertainties. The fluctuations could be perturbation of the compressor operating condition, or unsteady flow in the main gas path surrounding the turbine blades, or opening and closing of movable vanes in the compressor, or bleed valve scheduling, etc.

Traditional 1-D design tools are based on flow networks of pressure chambers and flow resistors. The tools require inputs from pressure loss to swirl ratio of the components. The accuracy of the prediction largely depends on how good are the estimations of the pressure losses and swirl ratios. The tools could provide good predictions if they were “validated” or data matched. However, for brand new designs, such as the configurations of impellers in this case, there is no previous experience to draw from and the 1-D design tools do not have enough fidelity to provide predictions with the necessary accuracy. For instance, the 1-D tools can neither distinguish the differences among the inlet angles and their associated losses nor correctly estimate the swirl ratio upstream of the impellers.

With the advancement of computer technology and maturity of numerical technique, CFD analysis has become a main stream analytical tool and has been widely applied to jet engine early design stages to gain insight before investing heavily in experimental demonstration [1]. In the high speed rotating turbomachinery environment, CFD is the best analytical tool available at present to evaluate impeller designs. As mentioned above, traditional 1-D tools do not have enough fidelity to account for detailed geometry changes and to estimate the impeller effects, while experimental measurements of pressure quantities in a highly rotating system are very difficult and expensive. CFD analysis can serve as a numerical rig for concept exploration and trending search. It is relatively inexpensive in comparison to hardware test and can provide insight of flow physics which is hard to obtain from the rig test.

Gupta et al [2] applied CFD simulations to a TOBI system and summarized design parameters of HPT disk with pumping vanes that can enhance pressure gain of the cooling air supply: effect of pumping vanes, effect of contoured vanes, effect of pumping vane solidity, effect of flow diffusion, effect of vane incidence angle, and effect of rim slot in the HPT disk.

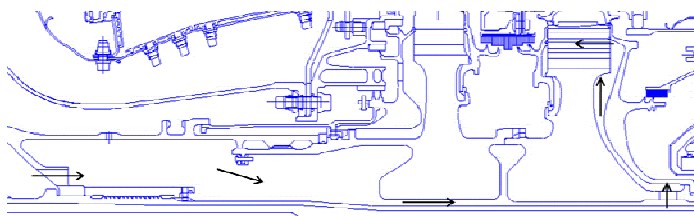


Figure 1 A 2-D schematic of the HPT cavities

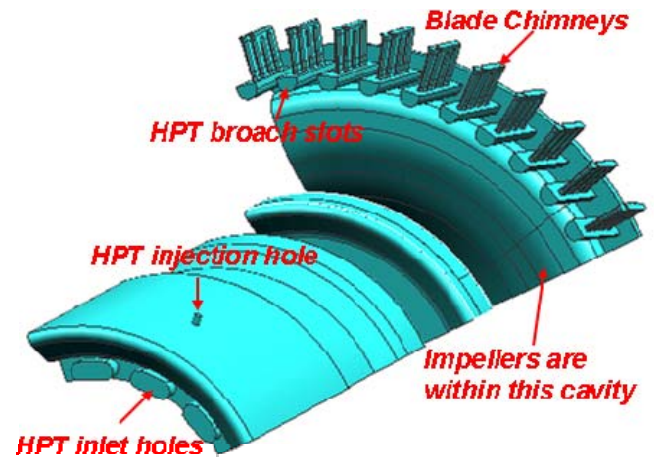


Figure 2 A 3-D Computational domain of HPT cavities

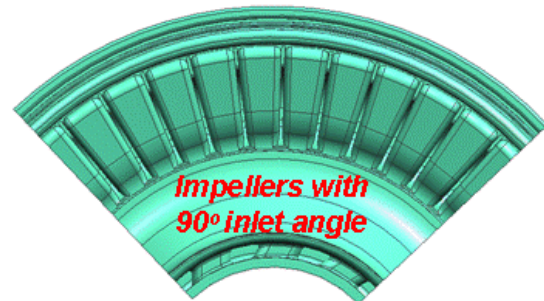


Figure 3 Example of 90 degree of inlet angle impellers on the minidisk, aft looking forward

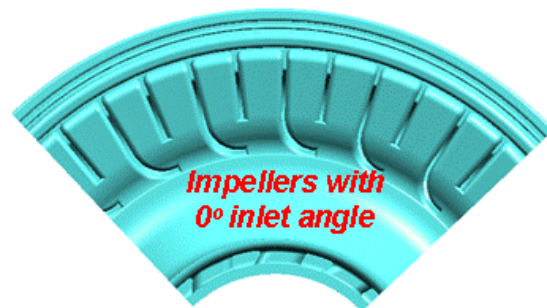


Figure 4 Example of 0 degrees of inlet angle impellers on the minidisk, aft looking forward

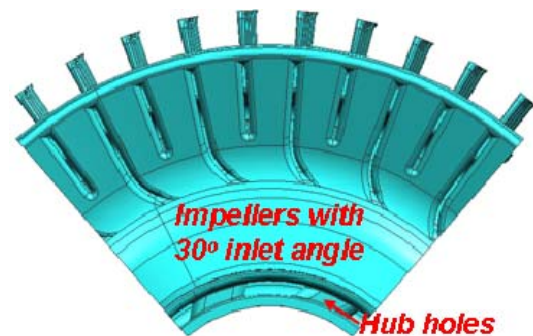
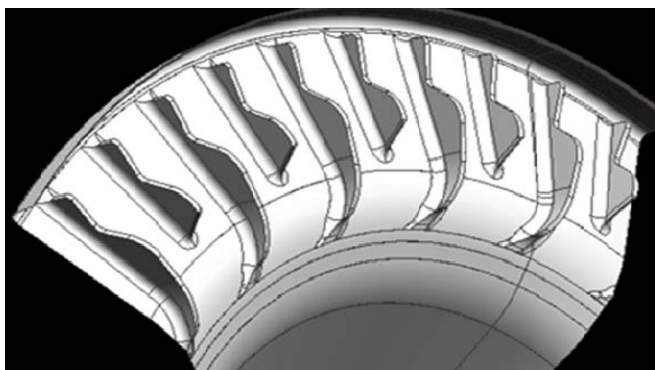


Figure 5 Example of 30 degrees of inlet angle impellers on the minidisk, aft looking forward



Impellers on the mini disk

Figure 6 A schematic of 30 degrees of inlet angle impellers passage within disk cavity

Reference [2] concluded the baseline straight pumping vane gained 4.6% of $P_{t \text{ inlet}}$ over the system without pumping vane. The contoured vanes can gain even more pressure rise. The impeller vane solidity is important to flow separation. The solidity is defined as C/s , the impeller chord divided by its spacing. The higher vane counts, the smaller spacing s and the higher solidity. For the 4x pumping vane solidity, meaning an arrangement of one pair pumping vanes for every 4 broach slots, the flow separation zone was quite large. The flow separation zone is reduced when the pumping vane solidity increased to 2x. Effect of impeller vane incidence angle plays an important role in pressure gain. Impeller vanes swept backwards reduces swirl ratio in comparison to vanes swept forwards. Flow diffusion plays a small role in gaining pressure rise. Rim slot is a very effective device since it increases flow swirl ratio before the flow gets on board the broach slot.

In this study, flow diffusion is not taken into design consideration since it is a less effective approach to achieve pressure gain. Structural integrity and weight concerns usually override the favorable aerodynamic shape of the cavity in turbine rotor design. The emphases are on high solidity impellers to minimize flow separation and on inlet and exit angles to effectively convert flow from a tangential direction to a radial direction.

The following three decisions were made at an early design stage after reviewing of the available literatures:

1) Choose the highest vane solidity possible. The CFD result in [2] shows that flow separation still exist within the pumping vane passage with 2x vane solidity. We have chosen the solidity of one pair of impellers per broach slot. The high solidity is aimed to suppress flow separation within the impeller passage and to achieve maximum pressure gain.

2) Choose impeller exit angle at 0° for the best effect of delivery flow to broach slots

3) Evaluate the best impeller inlet angle that also can be manufactured relatively easily and cheaply. The two extreme cases of impeller vane inlet angles at 0° and 90° were evaluated as the first step. The configurations are shown in Figures 4 and 3, respectively. Based on understanding of flow physics of these two extreme cases, a third configuration of impeller vane inlet angle at 30° , such as shown in Figure 5, was analyzed as a proposed design. This impeller configuration satisfies our requirements of both gaining high pressure and relative ease of manufacture.

2 COMPUTATIONAL DOMAIN

Figure 1 is a 2-D cross section of the computational domain that illustrates the cooling flow delivery system where arrows indicate flow path. The actual 3-D computational domain includes the HPT front and rear cavities, turbine blade broach slots and HPT blade chimneys, as shown in Figure 2. The computational model is the complement of the metal parts of the design and is called air solid. All air solids presented in the paper were made using the UG CAD package.

In reality, the flow field is a full 360° domain and fully unsteady. Project schedules and computational resources required to execute such calculations made it impractical to solve the whole domain unsteady. The approach used was to perform steady state CFD analysis with a partial sector model to capture the mean flow and pressure level more accurately than the traditional one-dimensional analysis. The sector model needs to take consideration the periodic requirement for the numbers of HPT inlet holes, the number of HPT injection holes and finally, the number of blades and impellers. The final computational model was an 81.82-degree sector which contains 5 pairs of impellers within the HPT cavity. Figure 5 is the air solid model of HPT cavity with impellers at 30° inlet angle where the rotating direction is clockwise, aft looking forward. Figure 6 is the same model but shows the detailed impeller design on the minidisk of the HPT rear cavity. The impeller depth follows the contour of the minidisk cavity with a tight clearance.

3 COMPUTATIONAL GRIDS

The computational grids were generated with the Ansys ICEMCFD grid generation package. The total cell counts are approximately 20 to 25 million for the HPT cavity model without and with impellers, respectively. Three prism layers were generated on all the solid walls to ensure appropriate resolution of a wall function type turbulence model. An example of grid at HPT inlet hole is shown in Figure 7. Due to the nature of very large computational models, an effort was made to apply fine grids where flow fields need to be resolved and coarse grids at areas with less flow activity. For instance, finer grids were used underneath the disk bore where prediction of friction loss is critical, while coarser grids are used in the middle of the HPT cavities. Also, mixed tetrahedron and hexahedron grids were used to reduce the total cell counts. Figure 8 displays a grid density arrangement at the straight impeller region.

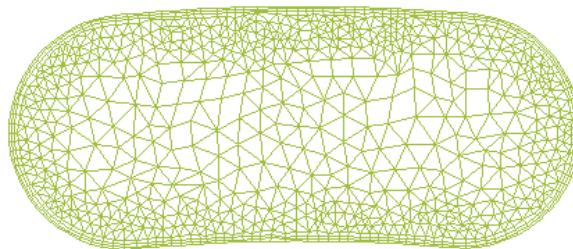


Figure 7 Example of mixed tetrahedron and hexahedron grids with prism layers at HPT inlet

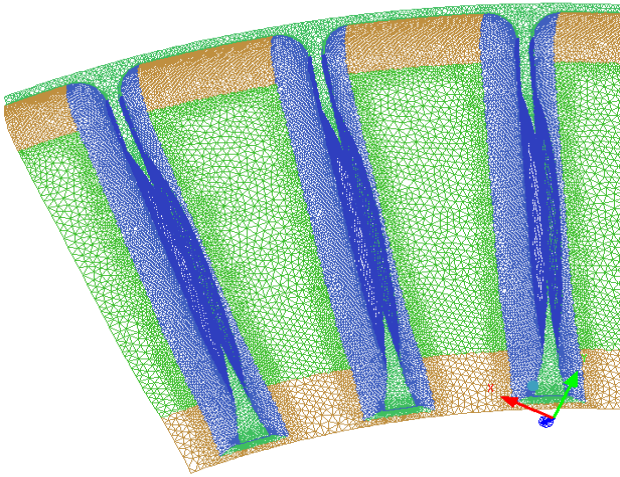


Figure 8 Example of grids density arrangement

Grid sensitivity study was conducted before the final decision on the grid was settled. The CFD computation of a wall integration type grid with 12 prism layers and $y^+ = 1$ was performed and compared to that of a wall function type grid with 3 prism layers and $y^+ = 100$. The difference of predicted system pressure losses between these two grids is less than 1%, indicating no gain of wall integration type grid probably due to a highly rotating but no major separation flow field. After considering the wall integration type grid for the same model is around 40-45 million cells that requires much more computer CPUs for execution and much larger disk space for storage, it is an easy decision to choose the wall function type grid with three prism layers.

4 COMPUTATIONAL BOUNDARY CONDITIONS AND SOLVER SETUP

The Ansys Fluent version 12 commercial CFD package was used for all CFD simulations. The computations were set to steady state in a single rotating reference frame. The single rotating reference frame can be applied to this particular problem since no stationary parts are involved in the model. The boundary conditions applied to the CFD model were fixed mass flow rate and total temperature at the inlets and fixed static pressure at the exits. The exit static pressure was adjusted until the inlet total pressure was matched to a given designed value. This approach correctly estimated exit static pressure at desired inlet total temperature, pressure and mass flow rate. If the exit static pressure is greater than desired blade supply pressure level, the configuration met design criterion. Otherwise, design changes were required to ensure the sufficient blade supply pressure level was reached.

The operating condition modeled was the engine at aircraft take-off condition, the non-dimensional flow rate C_w is 284931 and the rotational Reynolds number Re_ϕ is 15485667 [5] [6].

The turbulence model applied to the CFD computations in this paper were the standard $k-\epsilon$ two equation model with wall function approach.

The pressure-velocity coupled solver was chosen to ensure tight coupling between the momentum and energy equations. The coupled solver provides a better and quicker convergence for the diffusion dominated rotating flow field. The

convergence is judged by 3 criteria: 1) the residuals of continuity, momentum, energy and turbulence equations approach to flat lines; 2) the mass flow rate imbalance reaches a very small percentage of the total mass flow rate and 3) the changes of several monitored pressure values reach a small number. The solution is considered converged when all 3 criteria reach certain values. It usually takes 4000 to 5000 iterations to reach convergence for the typical steady state solution. It usually takes 4-5 days of computing time for each case to converge using 20 CPUs on a parallelized linux computer ring.

5 RESULTS AND DISCUSSIONS

HPT blade cooling air delivery systems with and without impellers were computed with identical inlet boundary conditions. Detailed attention was paid to ensure consistency in grid quality for all the models. The pressure differences of the two systems represent the effect of impellers.

Three non-dimensional parameters are used to evaluate the effectiveness of the impellers and the performance of the broach slots. β is the dimensionless ratio of swirl velocity versus disk wheel speed of the cavities (or so called RPM factor).

$$\beta = \frac{V_\phi}{\Omega r}$$

A β of unity means the tangential velocity of the cavity flow is the same as that of the disk wall. β less or greater than unity means flow tangential velocity rotates slower or faster than the disk wall, respectively.

ΔP_s is the normalized static pressure ratio of exit to inlet or static pressure coefficient. In this paper, ΔP_s is normalized by HPT inlet static pressure.

$$\Delta P_s = \frac{P_{se}}{P_{si}}$$

ΔP_s greater than 1 means static pressure gain from inlet to exit. Relative axial Mach number is defined as

$$Ma = \frac{V_a}{\sqrt{\gamma RT_s}}$$

A large relative axial Mach number within the broach slots suggests a large pressure loss.

5.1 EFFECT OF IMPELLER VANE INLET ANGLE

The baseline CFD analysis is for a cooling air delivery system without impellers. This is completed as the first step in order to establish a baseline system pressure loss. CFD analyses of a system with impellers are performed to evaluate the benefit of the impellers relative to the baseline configuration. For a system with impellers, a 0° vane exit angle and high solidity design of one pair of impeller per broach slot was chosen. The 0° vane exit angle guarantees the best swirl ratio matching for the cooling flow getting on board of the blade broach slots. It is believed that high solidity impellers would reduce flow separation within impeller passages.

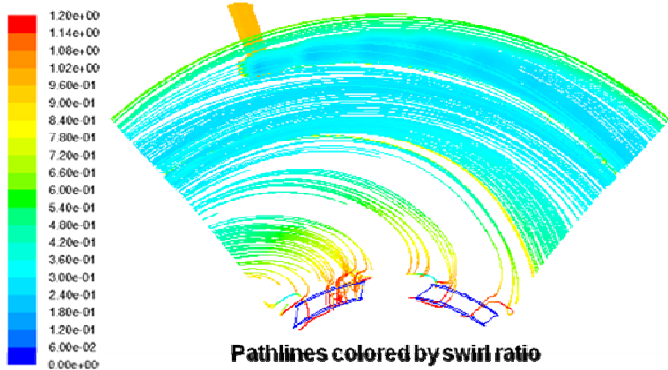


Figure 9 Flow pathlines from hub hole to broach slot of the baseline configuration

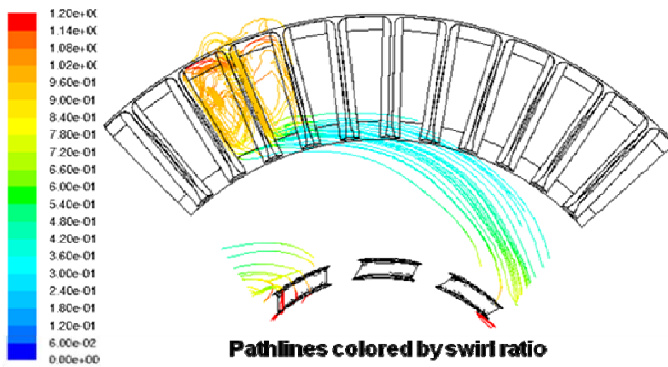


Figure 10 Flow pathlines from hub hole to broach slot of impellers with 90° vane inlet angle

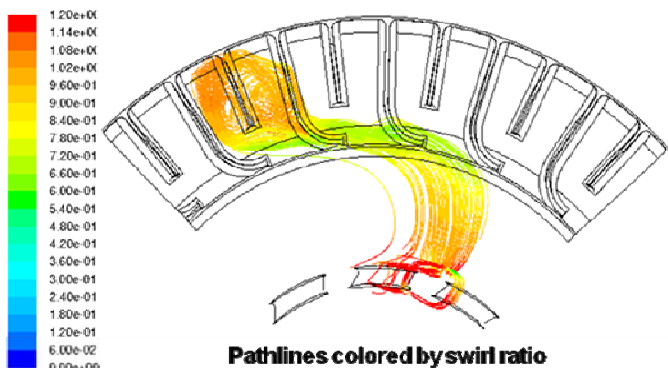


Figure 11 Flow pathlines from hub hole to broach slot of impellers with 0° vane inlet angle

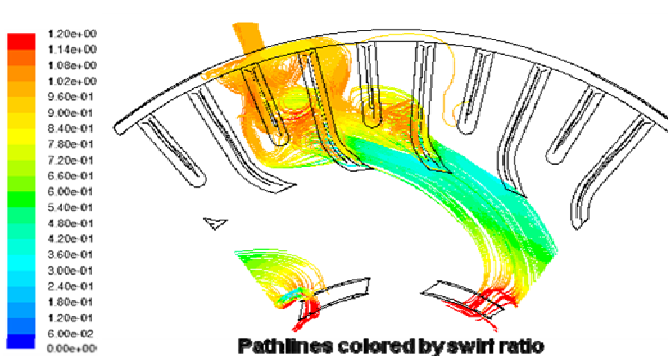


Figure 12 Flow pathlines from hub hole to broach slot of impellers with 30° vane inlet angle

A total of four CFD analyses were performed to evaluate the cooling air delivery systems without and with impellers. Besides the baseline, the other three configurations were at different vane inlet angles. The two extreme limits of vane inlet angle 0° and 90° were evaluated after the baseline configuration. 0° vane inlet angle means the entrance of the vane is parallel to the flow rotating direction. The impeller should have the best “scoop” effect and least entrance loss. On the other hand, 90° vane inlet angle implies the entrance of the vane is perpendicular to the flow rotating direction, therefore the impeller should have the least “scoop” effect and worst entrance loss. It is totally opposite in terms of manufacturing ability and cost. The 0° inlet angle impellers are the most difficult and expensive to manufacture while the 90° inlet angle impellers are relatively easiest and cheapest to manufacture. The fourth configuration, 30° inlet angle impellers are the proposed design balances good aerodynamics and ease of manufacture.

Figures 9-12 are CFD results from these 4 configurations. The figures present flow pathlines colored by swirl ratio or RPM factor. The flow pathlines are the fluid particle trajectories integrated from hub hole to one of the broach slot exits that are marked by swirl ratio level. The flow swirl ratio is between 0 and 1.2 for those 4 configurations after leaving the hub holes. The swirl ratio variations are caused by impeller inlet angle. Figure 9 presents flow pathlines for the baseline configuration. Without impellers installed inside the disk cavity, the fluid particles travel the longest distance before reaching broach slots. Figure 10 shows the flow pathlines of the 90° vane inlet angle case. Before fluid particles reach impellers, the trajectory is very similar the path of the baseline. After fluid particles reach the straight impellers, they are forced into impeller passages to feed the broach slots and the fluid particles travel the second longest distance. Figure 11 shows that the fluid particles travel the shortest distance from hub holes to broach slots at 0° impeller vane inlet angle. Another interesting observation from Figure 11 is that 0° vane inlet angle induces the highest swirl ratio at region upstream of the impeller entrance. As expected, for 30° vane inlet angle, Figure 12 shows the fluid particles travel the second shortest distance between hub holes and broach slots. By reviewing Figures 10, 11 and 12, the importance of impeller vane inlet angles is observed. The findings suggest that the impeller vane inlet angle affects the flow field both upstream and downstream of the impellers. The smaller the vane inlet angle, the better the flow is delivered to impellers, the highest swirl ratio is induced before flow reaches impellers, and the fluid particles travel the shortest distance from hub holes to broach slots.

5.2 EFFECT OF IMPELLERS INSIDE CAVITY

Figures 13 through 20 are used to further illustrate the swirl ratio and static pressure coefficient contour of the baseline configuration and three configurations with different impeller vane inlet angles. These 8 figures are taken at the mid- plane of HPT rear disk cavity to display distinctive aerodynamic flow patterns.

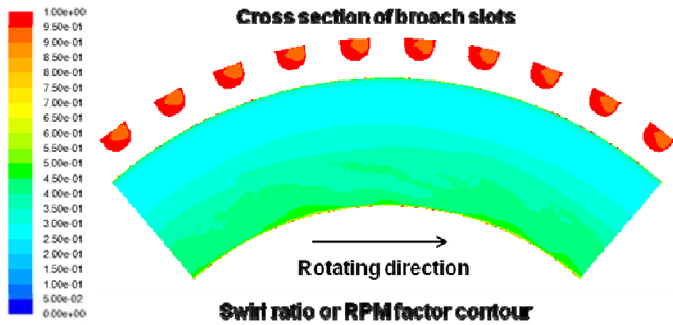


Figure 13 Swirl ratio of HPT cavity without impellers

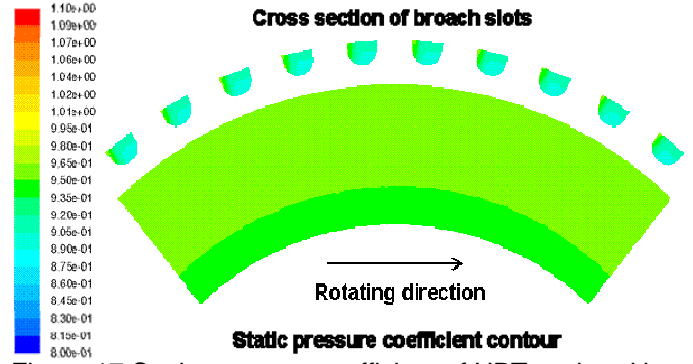


Figure 17 Static pressure coefficient of HPT cavity without impellers

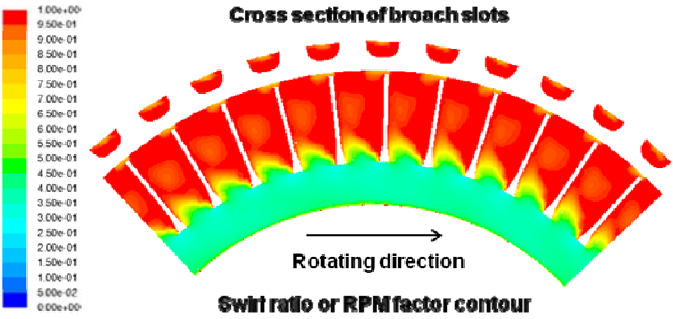


Figure 14 Swirl ratio of HPT cavity with impeller vane inlet angle at 90°

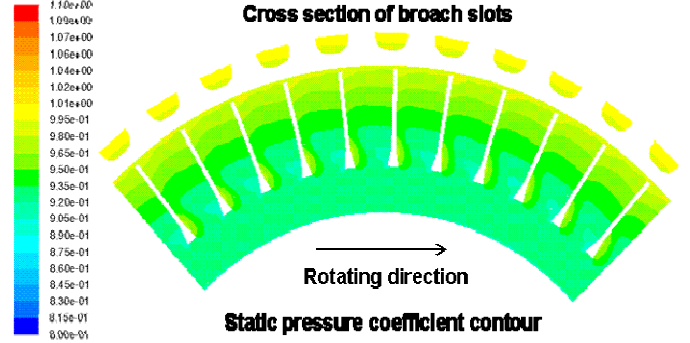


Figure 18 Static pressure coefficient of HPT with impeller vane inlet angle at 90°

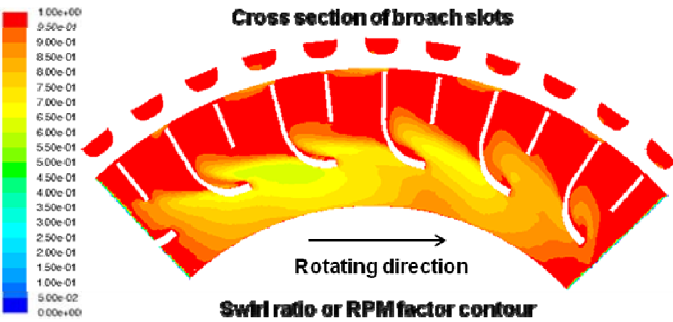


Figure 15 Swirl ratio of HPT cavity with impeller vane inlet angle at 0°

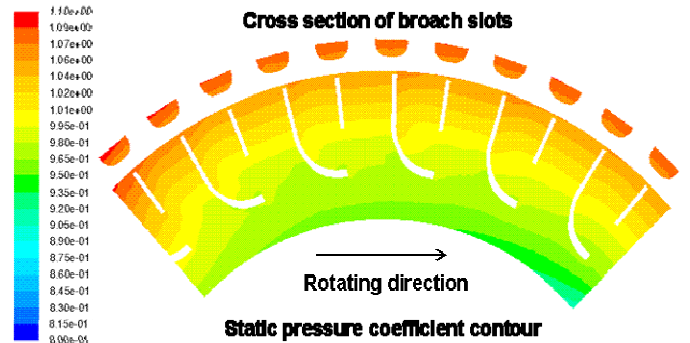


Figure 19 Static pressure coefficient of HPT cavity with impeller vane inlet angle at 0°

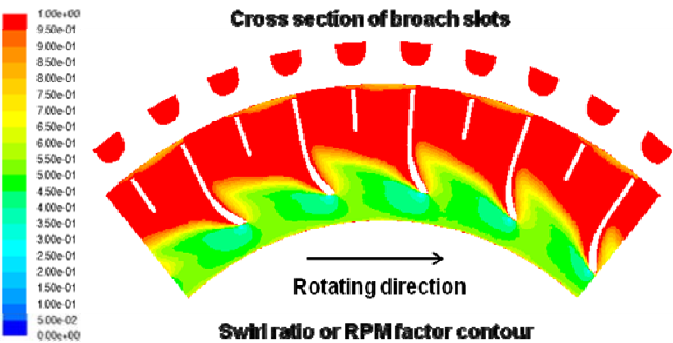


Figure 16 Swirl ratio of HPT cavity with impeller vane inlet angle at 30°

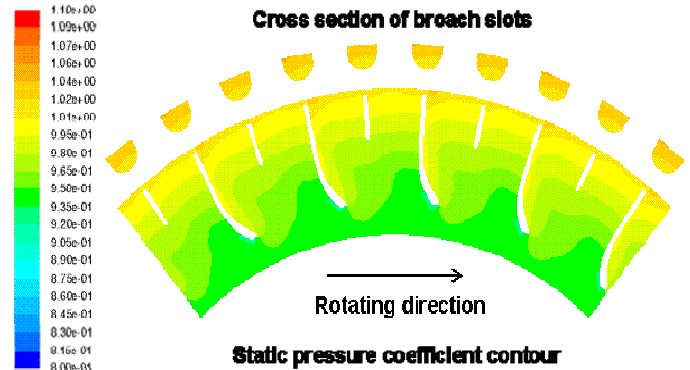


Figure 20 Static pressure coefficient of HPT cavity with impeller vane inlet angle at 30°

Figure 13 shows the swirl ratio within HPT cavity without impellers. After entering HPT rear disk cavity through the hub holes, the flow rotates at a tangential velocity that is far below the disk rotating speed, while flow within the broach slots rotates at swirl ratio close to 1. There is a fairly large disparity of swirl ratio between the flow within cavity and broach slots. Figure 14 presents the swirl ratio of impellers vane inlet angle at 90° . The large vane inlet angle induces lower swirl ratio upstream of the impellers and the straight impellers forced the swirl ratio to suddenly increase to unity at impeller entrance.

Figure 15 displays the benefit of reducing impeller vane inlet angle to zero degrees. When the vane inlet angle matches nicely with the flow rotating direction, flow is not being forced to change the direction and the swirl ratio is much higher upstream of the impellers. There is almost no swirl ratio disparity between flows midway through the disk cavity and within broach slots. Figure 16 is the swirl ratio of 30° impeller vane inlet angle, the overall performance trend shows this configuration is slightly worse than 0° vane inlet angle, but much better than that of 90° vane inlet angle.

Figures 17 through 20 present a direct comparison of static pressure pattern inside the HPT rear disk cavity of the four configurations. Figure 17 shows the lowest static pressure increase within the HPT rear cavity for the baseline. The most noticeable feature in Figure 17 is that the pressure within broach slots is lower than that within the HPT rear disk cavity and this implies a pressure loss from cavity to broach slots. Figures 18 to 20 present a different trend in static pressure contours. The static pressure increases with increasing radius of impellers and it is almost the same order when flow enters into broach slots. Among the three configurations, impellers with 0° vane inlets have the best performance, following by impellers with 30° and 90° vane inlet angles respectively. In general, the configuration with highest swirl ratio has the best static pressure increase.

As we discussed previously, the 30° vane inlet angle is the proposed configuration for a blade cooling air delivery system with impellers because it combines good aerodynamic performance and affordable manufacturing ability. The following discussion is only focused on the baseline configuration and the system with impellers at 30° vane inlet angle.

Swirl ratio and pressure increase can be quantified by integrating mass averaged swirl ratio and static pressure coefficient at various radii. Figure 21 presents the behaviors of swirl ratio versus normalized radius with and without impellers. Both systems have a swirl ratio of 0.81 at a normalized radius of 0.4, which is at the inner diameter of the HPT rear disk cavity. Due to the divergence of HPT cavity flow area, the swirl ratio decreases with the increasing of the cavity radius. The swirl ratio reduces to 0.4 at a normalized radius of 0.6 for both systems. From there on the two systems behave differently. The blue curve represents system without impellers. Swirl ratio keeps decreasing to 0.3 as the normalized radius increases to 0.86. The swirl ratio jumps to 1 as the flow enters broach slots. The red curve represents the system with impellers. Swirl ratio starts to increase as flow is scooped into bottom of impellers at a normalized radius of 0.6. The swirl ratio gradually increases to 0.98 within the impellers as normalized radius increases to 0.86. At that radius, flow enters into broach slots and swirl ratio becomes unity. The mass flow

rate averaged swirl ratio is slightly higher within the broach slots for the system without impellers than that of system with impellers due to impingement of the flow onto one side of the broach slots.

Figure 22 reveals the trends of the static pressure ratio versus the normalized radius of two systems with and without impellers. For both systems, rotational pumping within the HPT rear disk cavity generates static pressure gain from normalized radius 0.4 to 0.6. The system without impellers experiences about 2% increase in normalized static pressure ratio between the normalized radius of 0.6 to 0.86. At a normalized radius of 0.86, from where flow enters the broach slots, a large pressure drop occurs for the system without impellers that is equivalent to all the pressure gained within the HPT rear disk cavity. There is approximately 4.5% normalized static pressure ratio increasing within the blade chimney after flow enters broach slots. The system with impellers experiences a much larger pressure increase from a normalized radius 0.6 to 0.86 due to work done by impellers. There is a very small pressure drop as flow enters the broach slots. The static pressure keeps increasing about 8% inside the blade chimney after flow enters into the broach slots. It is noticeable that the system with impellers gains close to twice the pressure inside the blade chimney in comparison to the system without impellers. Over all, with static pressure at normalized radius of 0.4 as reference, the normalized static pressure coefficient increases 4.5% and 19% at the exit of the blade chimney for systems without and with impellers, respectively.

5.3 EFFECT OF IMPELLER ON BROACH SLOT

For a cooling air delivery system without impellers, the largest pressure loss occurs as flow enters into broach slots, which can be explained by further examination of the flow field. Two significantly different flow patterns for the systems with and without impellers are observed from the CFD solutions. Figures 23 and 24 represent two different types of flow trajectory. Figure 23 represents the system without impellers. The tangential velocity within HPT rear disk cavity is much slower than the broach slot rotating speed. There is a mismatch of swirl ratio or RPM factor at the entrance of the broach slots. Since the broach slots are rotating faster than cavity flow, the slow cavity flow impinges onto one side of the broach slot and creates large clockwise recirculation zones. In figure 24, the impellers force the cavity flow to change direction at a lower radius. The swirl ratio increases along the radius and is well matched at entrance of the broach slots. Therefore the flow is delivered into broach slots smoothly and without large recirculation zones. These two flow patterns can be clearly seen from a side by side comparison in Figure 25. The consequence of the large recirculation zones is a large pressure drop occurring at the broach entrance and overall lower static pressure within broach slots, as shown in Figure 26. The large recirculation zone also causes less pressure increase inside the blade chimney in comparison to analysis with impellers.

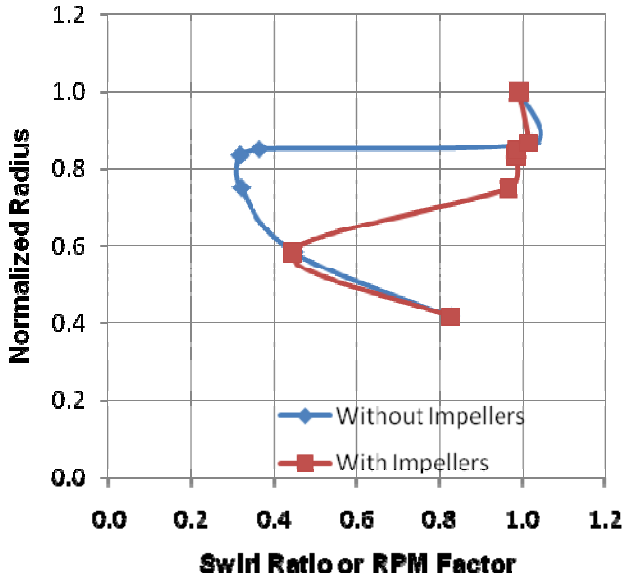


Figure 21 Comparison of HPT cavity swirl ratio increasing along radius, with and without impellers

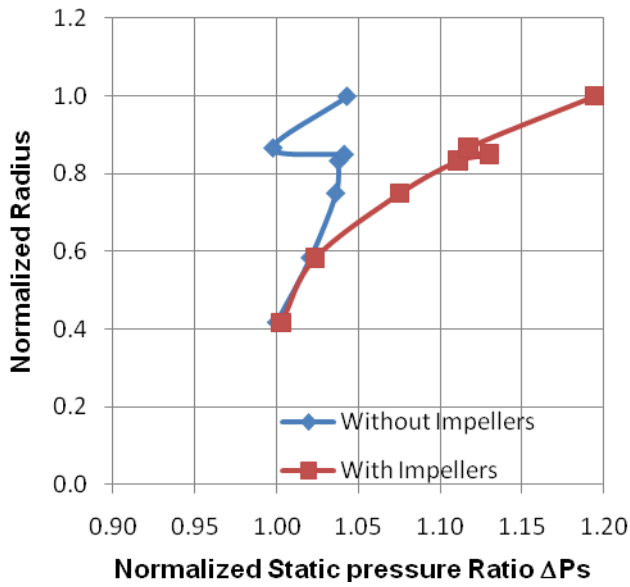


Figure 22 Comparison of HPT cavity pressure increasing along radius, with and without impellers

Figures 27, 28 and 29 are detailed comparisons of swirl ratio, relative axial Mach number and static pressure coefficient between systems with and without impellers at two reference planes within broach slots. The horizontal plane, in a top-view, is taken from a constant radius at the middle of the broach. The cross plane, in an aft-looking-forward view, is taken from a constant axial distance about one third inside of the broach slot entrance. For each figure, the left hand side is for the system without impellers and right hand side for system with impellers. The overall trend shows that the broach slot of the system with impellers behaves much better aerodynamically. The swirl ratio

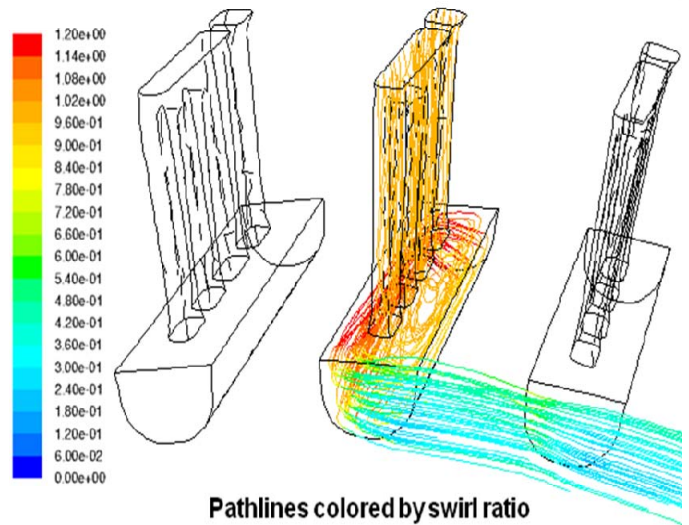


Figure 23 Pathlines of broach slots without impellers

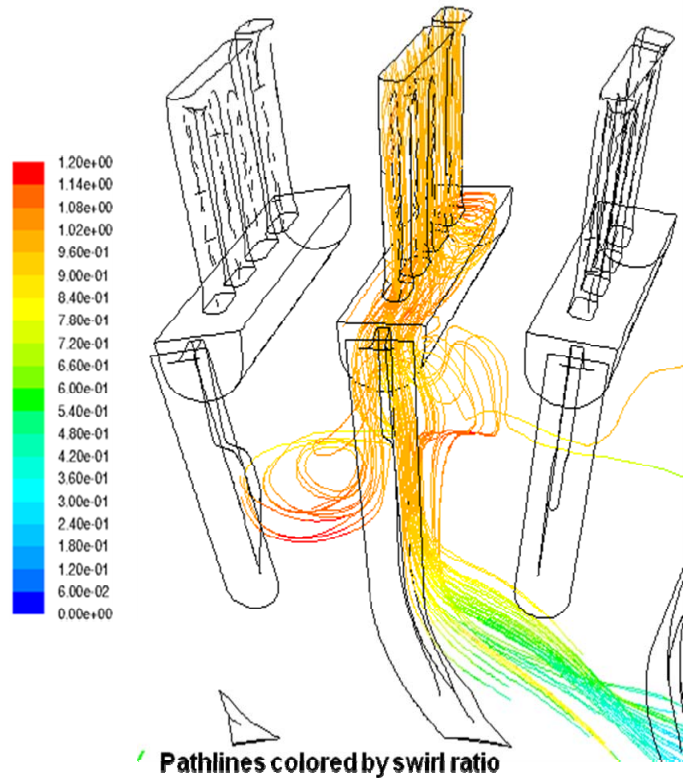


Figure 24 Pathlines of broach slots with impellers

is very uniform inside horizontal and cross planes, as shown in the right hand side of Figure 27. The same is true for the relative axial Mach number and static pressure coefficient at the right hand side of Figures 28 and 29. In general, when the flow swirl ratio matches well between cavity and broach slots, the flow is well behaved and the loss is small.

On the other hand, the left hand side of Figures 27, 28 and 29 show unfavorable aerodynamic behaviors in the broach slot for systems without impellers. In figure 27, it shows that the swirl ratio jumps from 0.3 to 1 at broach slot entrance. The mismatch of the swirl ratio at the entrance carries inside the

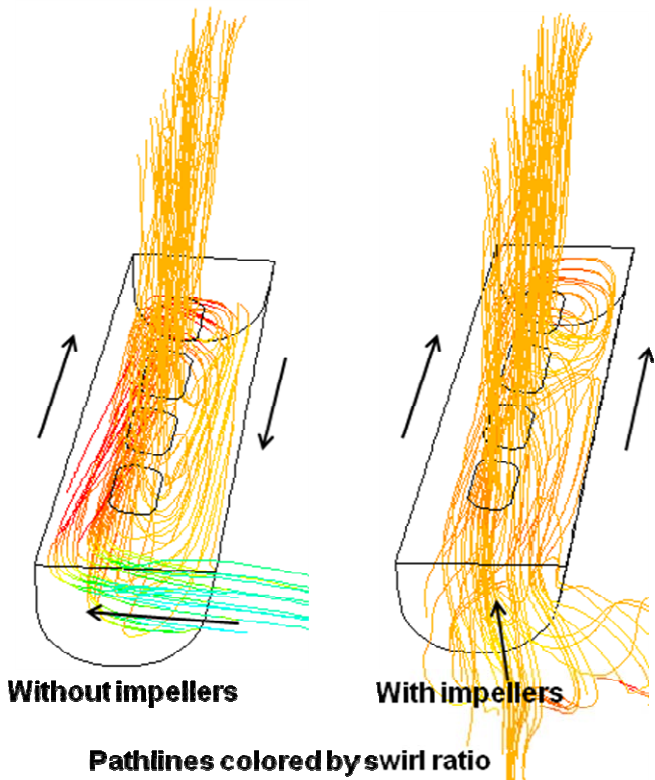


Figure 25 Comparison of broach slots flow feature with and without impellers

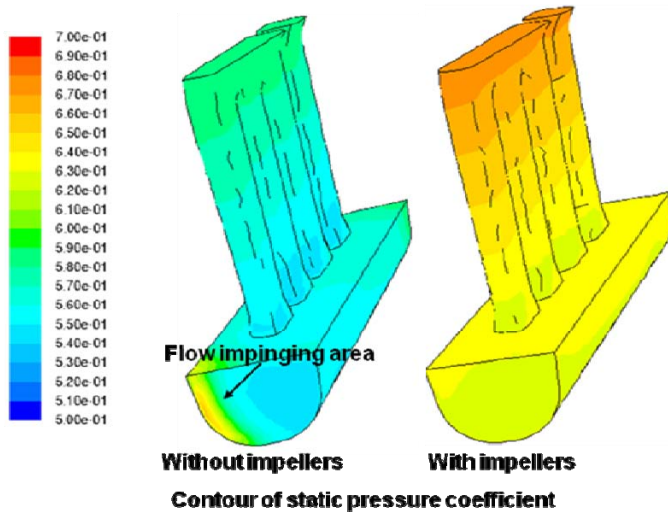


Figure 26 Comparison of static pressure of broach slots with and without impellers

broach slot and results in higher swirl ratio on one side than the other. Figure 28 shows the large clockwise recirculation zone as indicated by the large relative axial Mach number. The peak relative axial Mach number reaches 0.45 on the left side of the broach slot. The vertical layer type of structure seen from the broach slot cross section in Figure 28 represents the strength of the large recirculation zone. The flow pattern decides the static pressure distribution on the left hand side of Figure 29. The impinging flow from the disk cavity produces a very high static pressure zone at the left hand side corner while the strong large

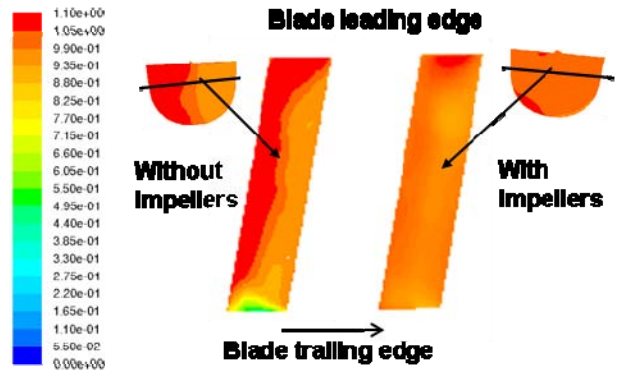


Figure 27 Comparison of swirl ratio of systems with and without impellers at broach reference plane

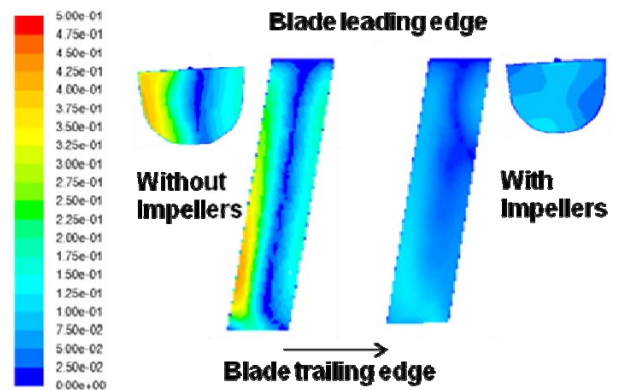


Figure 28 Comparison of relative axial Mach number of systems with and without impellers at broach reference plane

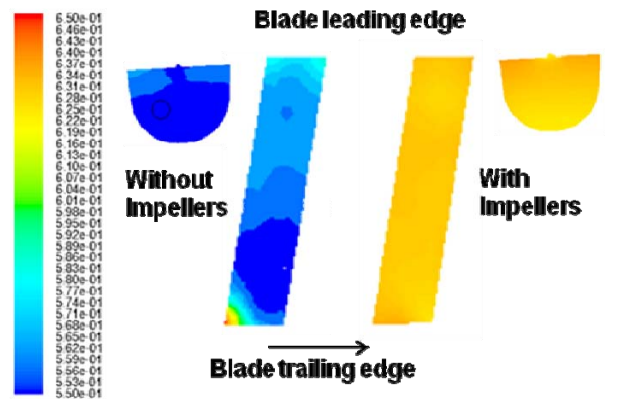


Figure 29 Comparison of static pressure of systems with and without impellers at broach reference plane

recirculation zone generates a low pressure region in the forward portion of the broach slot.

Favorable aerodynamic performance at the broach slots comes with prices. There is a manufacturing cost associated with machining impellers from the HPT rear cavity mini disk.

There are also structural integrity and weight concerns of installing impellers. The cooling air temperature is slightly higher for systems with impellers because of the higher temperature associated with higher pressure level. In addition, there is parasitic drag induced by impellers which results in an engine performance penalty.

This study provides us with the understanding of any device that eliminates or reduces large recirculation zones within broach slots will help improve broach slot aerodynamic performance and increase pressure gain within the blade chimney. For instance, impellers can eliminate swirl ratio mismatch at broach slot entrance, rim slots can reduce swirl ratio mismatch at broach slot entrance[2], and deflectors can reduce large recirculation with broach slots[3] [4].

6 CONCLUSIONS

CFD analyses were performed to evaluate supply pressure levels for two HPT blade cooling air delivery systems. The baseline was a system without impellers, and the alternative was a system with high solidity impellers at three various inlet angles and 0° exit angle.

The three various vane inlet angles are at 0°, 30° and 90° for system with impellers, respectively. These three configurations were evaluated before choosing 30° vane inlet angle as the best candidate. This configuration combines good aerodynamic performance and relatively affordable manufacturing cost.

By comparing swirl ratio, relative axial Mach number and static pressure coefficients of the two systems, it was found that the baseline configuration was less effective in gaining pressure rise within HPT rear disk cavity and blade broach slot. The analysis suggests that the design without impellers produces less pressure rise in the disk cavity and a larger entrance pressure loss due to the mismatch of the swirl ratio at the entrance of broach slot. Also the flow inside blade chimney gains less pressure increase due to a large recirculation zone caused by the mismatch of the swirl ratio at the broach slot entrance.

Design is a process of compromise. A system without impellers delivers less-desirable pressure distributions at blade root but has a lower manufacture cost. A system with Impellers provides favorable aerodynamic performance at the blade root that results in large pressure increasing for higher supply pressure, but at higher manufacture cost, extra weight, disk structure and stress concerns and lower TSFC due to parasitic drag. Since both systems satisfying the supply pressure

requirement, the final choice is the low manufacture cost design.

7 ACKNOWLEDGEMENT

The authors are thankful to Pratt & Whitney for granting the permission to publish this work. The authors would also like to express their gratitude to Mr. Daniel Lecuyer of Pratt & Whitney Canada for providing the impeller designs.

REFERENCES

- [1] Snowsill, G.D. & Young, C., 2006, "The Application of CFD to Underpin the Design of Gas Turbine Pre-swirl Systems", ASME Turbo Expo 2006, ASME Paper GT2006-90443.
- [2] Gupta, A.K., Remerth, D. & Ramachandran, D., 2008, "Numerical Simulation of TOBI Flow – Analysis of the Cavity between a Seal-Plate and HPT Disk with Pumping Vanes", ASME Turbo Expo 2008, ASME Paper GT2008-50739.
- [3] Ennacer, M., Guevremont, G., Djeridane, T., Sreekanth, S. & Lucas, T., "Blade Air Cooling Feed System CFD Analysis and Validation", ASME Turbo Expo 2007, ASME Paper GT2007-27002.
- [4] El-Sadi, H. Guevremont, G., Marini, R. & Girgis, S., "CFD Study of HPT Blade Cooling Flow Supply Systems", ASME Turbo Expo 2007, ASME Paper GT2007-27228.
- [5] Owen, J.M and Rogers, R.H., 1989. "Flow and Heat Transfer in Rotating-Disc Systems, Volume 1 – Rotor-Stator Systems". Research Studies Press LTD, Taunton, Somerset, England and John Wiley & Son Inc, New York, USA.
- [6] Owen, J.M and Rogers, R.H., 1995. "Flow and Heat Transfer in Rotating-Disc Systems, Volume 2 – Rotating Cavities". Research Studies Press LTD, Taunton, Somerset, England and John Wiley & Son Inc, New York, USA.